

IV. Department of Engineering and Technical Services

The Department of Engineering and Technical Services is involved in a wide range of work in the design, fabrication, construction, and operation of experimental devices in the fields of software and hardware.

This department is composed of engineers, and their tasks fall under the following five goals:

- 1) To develop advanced and systematic engineering capabilities on the basis of basic engineering results which have been obtained thus far.
- 2) To nourish excellent engineers.
- 3) To cultivate creative engineering abilities and skills.
- 4) To improve the documentation and the transfer of engineering knowledge to the next generation.
- 5) To perform tasks.

The department consists of the following five divisions. The Fabrication Technology Division oversees the construction of small devices and quality control of parts for all divisions. The Device Technology Division works on the Large Helical Device (LHD) and its peripheral devices except for heating devices and diagnostic devices. The Plasma Heating Technology Division supports the ECH system, the ICRF system, and the NBI system. The Diagnostic Technology Division develops, operates, and maintains all diagnostic devices. And the Control Technology Division concentrates on the central control system, the cryogenic system, the current control system, and the NIFS network. The total number of staff is 46 engineers and 12 part-time workers. We take care of the development, the operation, and the maintenance of the LHD and its peripheral devices with approximately 46 engineers.

1. Fabrication Technology Division

The main work of this division is the fabrication of experimental equipment. We also take care of technical consultation and experimental parts supplies related to the LHD experiment. In addition, we manage the administrative procedures of the department.

The number of fabrication requests was 175, and the total number of production parts was 675 during this fiscal year (FY). The total numbers of electronic engineering request and article are 22 and 37, respectively. The details of some of this division's activities follow below.

(1) The high speed AD converter

The prototype of the 12bit 500MHz sample/sec 1ch AD converter circuit for the Thomson-scattering diagnostics was composed of the 3 kinds of the computer boards. These boards are AD converter (ADS5463, Texas Instruments) (see Figure 1), FPGA (Spartan6, Tokuden) and Silicon TCP/IP (SOY-GbE, Bee Beans Technology). As a result of the operation test, this converter can transport the stored data in the memory of FPGA from this system to a PC through

the Ethernet LAN. In the next step, the converter will have one more AD channel, and the entire circuit will be integrated into a single board.

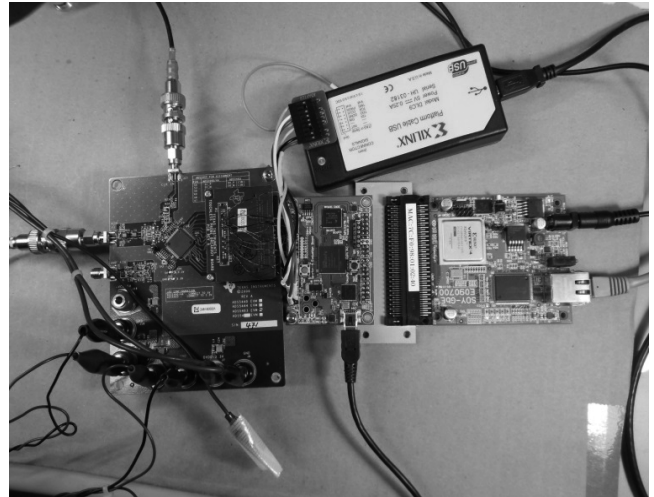


Fig. 1. Prototype of the high speed AD converter.

(2) Oxygen-free copper shield box for the quench detector

We manufactured 13 oxygen-free shield boxes by TIG welding. The shield box is welded oxygen-free copper of thickness 2mm by TIG welding. (Fig. 2) It is difficult to weld oxygen-free copper because the heat conduction is high. We spent much time training to weld oxygen-free copper. We used a shielding gas that is a mix of argon and helium. The shielding gas gave us the most suitable welding condition.



Fig. 2. Oxygen-free copper shield box.

(3) Corner bend

A corner bend is one of the waveguide components for the microwave transmission line. It is used for bending a corner at a right angle. The inside dimension of the rectangular waveguide fits the X-band microwave whose frequency range is 8.2 - 10.4 GHz. There are two types of design. One is 10.2 mm in height and 22.9 mm in width, and the other is 22.9 mm in height and 10.2 mm in width. The first type is bent along the electric field plane of the transmission

microwave in the waveguide, and the other type is bent along the magnetic field plane. The material is an aluminum alloy. We made 90 corner bends (see Figure 3) using the machining center.

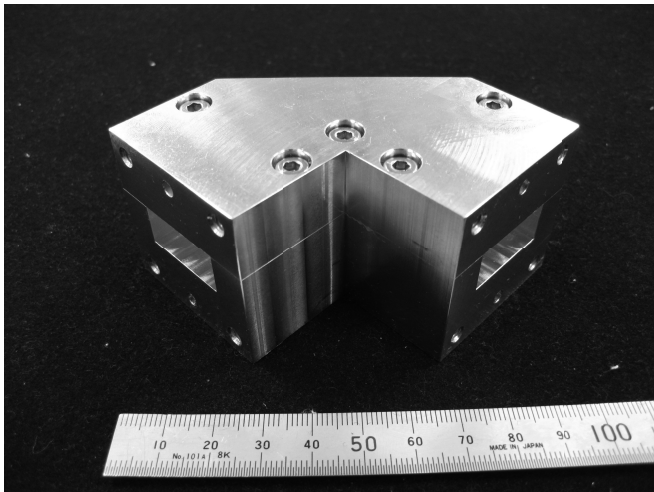


Fig. 3. Corner bend.

2. Device Technology Division

The Device Technology Division supports the operation, the improvement, and the maintenance of the LHD.

(1) Operation of LHD

We began the evacuation of air from the cryostat vessel for cryogenic components on September 16, 2014, and from the plasma vacuum vessel on September 17. Subsequently, we checked air leaks from the flanges of the plasma vacuum vessel. The number of checked flanges was 100. As a result, there was no leak. The pressure of the cryostat vessel achieved the adiabatic condition ($< 2 \times 10^{-2}$ Pa) on September 19 and the pressure of the plasma vacuum vessel reached below 1×10^{-5} Pa on September 29.

The LHD experiment of the 18th experimental campaign began on November 6, 2014, and continued until February 2, 2015. The number of days of the plasma experiment was 44 in total.

During this experimental campaign, the vacuum pumping systems were able to evacuate both of the vessels without any trouble. The LHD operation was completed on February 26, 2015.

(2) Renewal of the gas supply system for the D₂ plasma experiments.

The gas supply system was renewed to correspond to the plasma experiments that will use deuterium (D₂).

We must move all gas cylinders in the gas supply system from the experiment room to another room before the D₂ plasma experiments, because it will be difficult to remove articles in the experiment room during the D₂ plasma experiments.

This gas supply system is operated as the gas utility that can supply several kinds of gas to several devices in the experiment room.

The gases that this system can supply are Ar, H₂, He, D₂, Ne, N₂ up to 0.2MPa or 8MPa, and other special gases (Kr, Xe, etc.) up to 0.2MPa. The pressure of Ar, He, Ne, and N₂ can be boosted by a compressor if the pressure of a gas cylinder falls below 8MPa. The impurity density of H₂, He, and D₂ is below 100 ppb, and that of Ar, Ne, N₂, and special gases is below 100 ppm in this gas supply system.

We had to dispose of some gas to exchange the supply gas in the previous gas supply system because the number of piezo valves and mass flow controllers were less than that of the kind of supply gas. It is not allowed to dispose of gas in the D₂ plasma experiments. For that reason, we increased the number of piezo valves, and mass flow controllers were fixed for the kind of the gas. We increased the number of piezo valves from 10 to 25 and the number of mass flow controllers from 2 to 12. (Figure 4).

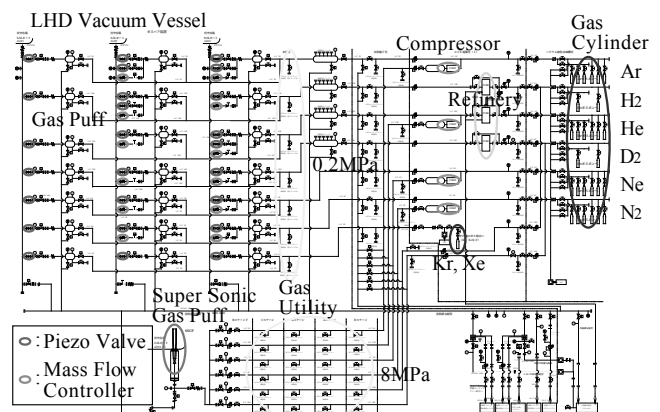


Fig. 4. New gas supply system

(3) Development of the improved cryo-sorption pump for the closed helical divertor in the LHD

Improvement of the particle pumping efficiency in the cryo-sorption pump installed in the Closed Helical Divertor (CHD) is an urgent task in the LHD. Thus, the improved cryo-sorption pump, which is installed in the dome structure, has been developed. Cross-sections of the previous type and of the improved type cryo-sorption pumps are illustrated in Figure 5. The cryo-sorption pumps are installed on the inboard side of the torus. In the improved cryo-sorption pump (see Figure 5(b)), two cryo-sorption panels cooled by gas helium (< 20 K) lie behind the dome structure for maximizing the pumping area. The Liquid Nitrogen (LN₂)-cooled blinds are inserted between the cryo-sorption panels and the vessel wall with room temperature (> 300 K). The LN₂-cooled panel installed in the central part increases the aperture area of the LN₂-cooled blinds. The water-cooled shield shades the LN₂-cooled components from the divertor plates, whose temperature reaches more than 1,300 K during plasma discharges. By concealing the cryo-sorption panel and the LN₂-cooled components along the back side of the dome, the line of sight from a strike-point on the divertor plate to the LN₂-cooled components can be interrupted. Therefore, the water-cooled blinds in Figure 5(a) are not needed. As a result, the exhaust conductance becomes large, and the pumping efficiency is improved.

The activated carbon bonded on the cryo-sorption panel has the adsorption property of hydrogen below 20 K. The

pumping performance is affected by the adsorption and desorption characteristics, which can be evaluated by measuring the pore size distribution. The pumping capacity and the pumping speed are determined by the micro-pore volume (pore diameter: 0.4-2 nm) and the meso-pore volume (pore diameter: 2-50 nm), [see Ref. 1) below], respectively. From the measurement of the pore size distributions in several kinds of activated carbons (shown in Figure 6), Shirasagi GH2X4/6 was selected as the activated carbon of the improved cryo-sorption pumps.

The activated carbon is generally bonded with the organic adhesion material on the cryo-sorption panel. However, the organic adhesion causes separation of the activated carbon by age deterioration, and regular maintenance is essential. Moreover, the organic adhesion causes the undesired gas release in the vacuum vessel during a non-cooling phase. Accordingly, an adhesion process with an indium solder has been established, and we succeeded in adhering the activated carbon to the cryo-sorption panel metallicity.

In this way, the test pieces of the cryo-sorption panel, as shown in Figure 7, have been made by using selected activated carbon and the adhesion process described above. Subsequently, we made the mock-up of the cryo-sorption pump, which simulates the positional relationship of the neighboring divertor plate, wall, and an integrated type dome structure, as illustrated in Figure 8. The pumping speed and the pumping capacity have been measured in the test-stand set-up for evaluating the pumping performance for hydrogen. The pumping performance evaluation test shows that the pumping speed in the improved pump ($6.4\text{m}^3/\text{s}$) is higher than that in the previous pump ($3.3\text{m}^3/\text{s}$) by a factor of approximately two. In addition, the pumping capacity in the improved pump ($7,880\text{ Pa m}^3$) is higher than that in the previous pump ($1,910\text{ Pa m}^3$) by a factor of approximately four.

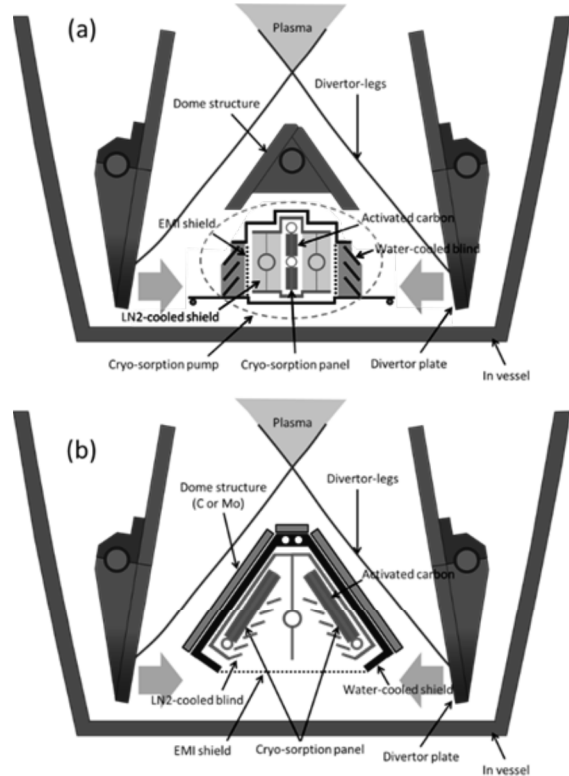


Fig. 5. Cross sectional views of (a) the previous type and (b) the improved-type cryo-sorption pumps.

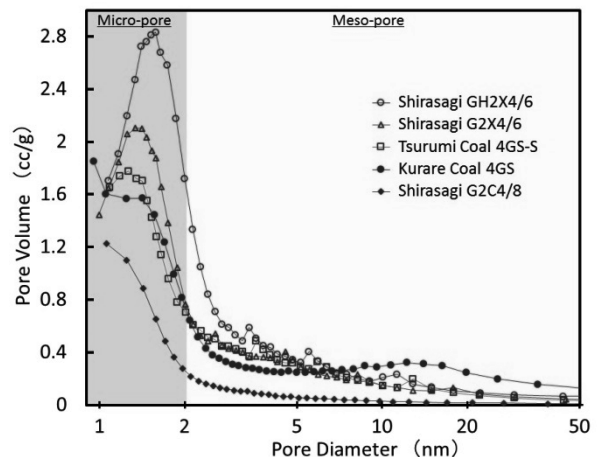


Fig. 6. Distribution of the pore volume in several activated carbons.

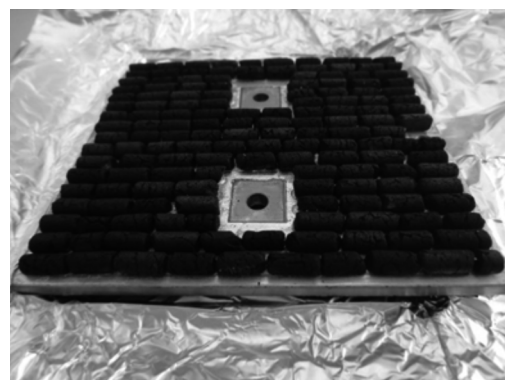


Fig. 7. Test piece of the cryo-sorption panel made by using the adhesion process with an indium solder.

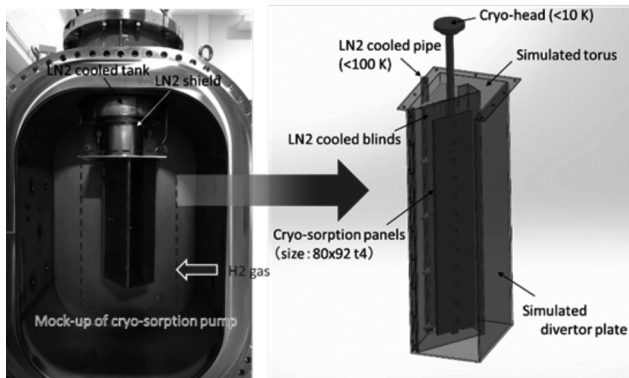


Fig. 8. A mock-up of the cryo-sorption pump with simulated torus and divertor plates.

1) Hayashi, M. et al, *Activated Carbon*, Maruzen, (2011) 377-450.

(4) The tritium monitoring measurement of the exhaust (the tritium sampler system II)

We are monitoring the tritium concentrations in the stack by the tritium sampler system. During this term, another tritium sampler system was installed to conduct the continual tritium concentration monitoring in the stack during the plasma experiment. The sampled air is collected by both tritium sampler systems. The old system to collect the tritium was separated in three chemical forms, but the new system can collect the tritium by gathering all chemical forms. The schematic diagram of the new tritium sampler system is shown in Figure 9. Now we are investigating the validity of the measurement results.

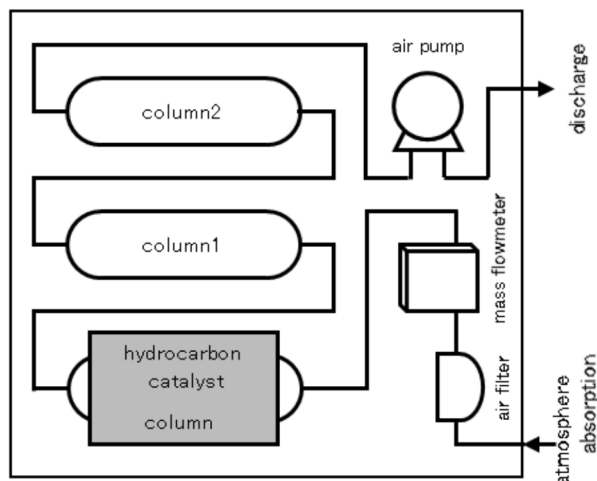


Fig. 9. The flow chart of the new tritium sampler system II.

(5) The test of the tritium monitor at the outdoor exhaust pipe

During the last fiscal year, the pressurized ionization chamber was installed at the outdoor exhaust pipe for exhausting the gas from the LHD to outdoors, and was checked regarding whether we could use it as a tritium monitor. As a result of the test, it was shown that the pressurized ionization chamber could not be used because

background data were not stable for it was affected strongly by the change of the radon density in the exhaust gas. In this fiscal year, we installed the gas-flow proportional counter, and checked whether we could use it as a tritium monitor. The β -ray emitted from tritium which has a very short range can be detected by this counter. Additionally, this counter has higher sensitivity than the pressurized ionization chamber because tritium can be detected separately from other nuclides. The test showed that the variation of the background data by the change of the radon density in exhaust gas could not be detected. Thus, we decided to use this tritium monitor.

3. Plasma Heating Technology Division

The main tasks of this division are the operation and the maintenance of plasma heating devices and common facilities. We have also performed technical support for improving, developing, and installing these devices.

In the 18th experimental campaign, a new 1 MW class output gyrotron at 154 GHz was installed in the ECH system, in addition to four 1 MW gyrotrons. The waveguide transmission lines and antenna system are modified so to inject the power by two-line connection to the U-port and four-line connection to the O-port. As a result, simultaneous injection power from an 82.7 GHz, three 77 GHz, and two 154 GHz gyrotrons reached approximately 5.6 MW. As for the ICH, the six antennas of the LHD were operated at the frequency of 38.47 MHz in this campaign. Total injection power reached 4.5 MW at maximum and about 1.5 MW in CW. As for the NBI, the ion sources of BL-2 and BL-3 suffered from vacuum leak problems during the experimental campaign, but the injection power reached 27.4 MW. The high voltage power supply for BL-4 was remodeled and the test operation at 60kV was performed. The motor generator (MG) supplied electric power stably and reliably to ECH in addition to NBI.

The details of these activities are as follows below.

(1) ECH

(a) Gyrotron Operation and the LHD experiment

During the 18th experimental campaign, we increased the total injection power to more than 5.6MW by the new 154GHz/1.2MW gyrotron that was installed. We injected ECH power stably during the whole campaign without any severe troubles that required a stop of operations for several days to restart. Figure 10 shows the results of injection power, which is the highest value in that day during this campaign. The highest power 5.6 MW is a record since we began operation. The low power injection means continuous wave (CW) operation. This operation contributes highly to the CW experiment that is shown by the achievement of approximately 41 minutes injection by these gyrotrons.

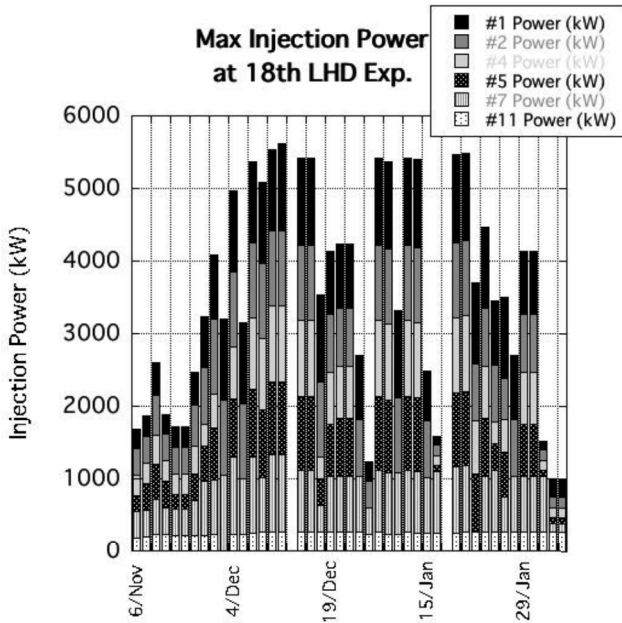


Fig. 10. Highest injection power of ECH in the 18th experimental campaign.

(b) Installation of two sets of new horizontal launchers

The ECH launchers installed in the 2O port, shown in Figure 11, have multiple mirrors with cooling systems. Each of the mirrors is made of aluminum alloy (A5052) and has a cooling water channel on the rear surface. In order to connect the channels of the mirrors with the cooling water pipes, we adopted friction pressure welding joints made from stainless steel (SUS316L) and aluminum (A1050). The design of the pipe route was complicated by the consideration of interference with other instruments. However, the pipe route was arranged efficiently by utilizing a 3D-CAD system.

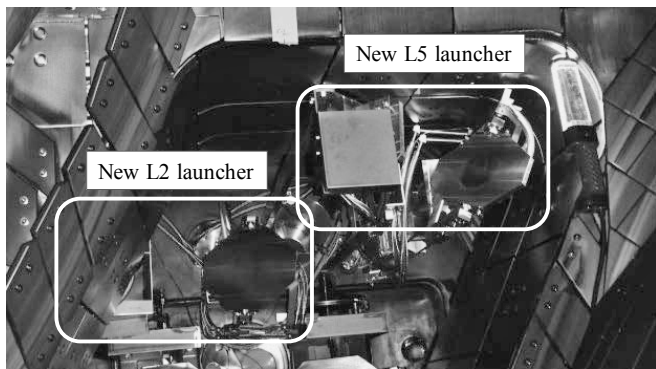


Fig. 11. 2O port with the new launchers.

(c) Challenging the feedforward control of the polarizers

A pair of $\Phi_{1/4}$ and $\Phi_{1/8}$ polarizers are set in each waveguide power transmission line for the ECH system and used for polarization control of EC-waves. We replaced all of the previous polarizers with the rotation speed of 12deg/s with new polarizers with the rotation speed of 180deg/s before the 18th experimental campaign. We usually used all the new polarizers in the 100deg/s setting. Our goal is to conduct feedback experiments of the polarizers in a pulse

discharge every few seconds. As the first step, for the purpose of confirming the feasibility of the feedback experiment, we carried out the feedforward experiment, in which the special apparatuses for the feedback experiment were not needed. We normally used the transmission control computer to control the polarizers, the antennas, etc. We connected a PC to the LHD-ECH controlling network. We prepared the order text file and the feedforward software to the computer. The feedforward software confirms the polarizer rotations according to the order, and sends the next order. Figure 12 shows traces of the polarization state realized by two consecutive shots. In the first shot, polarizers moved to $\alpha=0$ deg., $\beta=0$ deg. from $\alpha=-45$ deg., $\beta=0$ deg. Here, α and β denote the polarization angle and ellipticity, respectively. In the second shot, polarizers moved to $\alpha=45$ deg., $\beta=0$ deg. from $\alpha=0$ deg., and $\beta=0$ deg. It took 1.2 seconds to change the polarization in one shot. The system has enough rotation speed for the feedback experiment in LHD. But there are two problems. One problem is an old PC (Pentium) for controlling the polarizers. The other problem is the logging method of the polarizer position information. We will consider how to take encoder signals in a measurement device.

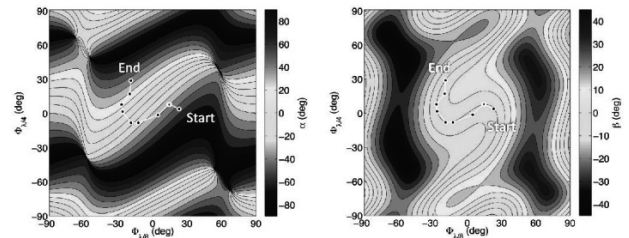


Fig. 12. Variation of polarization states, α and β , realized by the rotation angles $\Phi_{1/4}$ and $\Phi_{1/8}$ of the polarizers in the feedforward experiment

(2) ICH

(a) Operation and LHD experiment

In the 18th experimental campaign, we carried out the LHD experiment with six ICRF antennas and six RF oscillators with the fixed wave frequency (38.47 MHz). A noteworthy difference from the earlier experiments is that we cut and removed the Faraday shield of the 7.5L antenna similar to the 7.5U antenna. The total injection power with the six antennas into the plasma reached 4.5 MW in the short pulse length of 0.13 seconds and 1.34 MW in the 1294 seconds discharge. However, a water leak occurred in the 7.5L antenna during a steady state discharge later in this experimental campaign. Thereafter, we carried out a steady state discharge using four antennas, excluding the 7.5U and 7.5L antennas. Consequently, the injection power reached 2.05 MW in 193 seconds.

(b) Improvement of the gas cooling system for ceramic feedthrough

In order to cool the ceramic feedthrough during a steady state discharge, we have blown nitrogen gas on to the ceramic surface on the atmospheric side. The gas is sent to the feedthrough through the hose for supply from the

Heating Power Equipment Room, and is removed through the inside of the transmission lines connected with the feedthrough to the Heating Power Equipment Room. However, the nitrogen gas of about 0.3 MPa must always be filled between the inner conductor and the outer conductor of the transmission line during the power injection. Therefore, we must operate the valves for supply and venting while maintaining the filling pressure of the gas. Before the 18th experimental campaign, the staff of the ICRF group was busy with the operation of the valves at the Heating Power Equipment Room. Thus, we tried to improve the operation system of the valves. We adjusted the following three items.

- i) All of the exiting valves were changed to solenoid valves for making remote control possible.
- ii) A check valve was attached to the exit side of the solenoid supply valve.
- iii) Compact Field Point was used for control of the solenoid valves, and we developed the control panel using LabVIEW. The data of the gas pressure inside the transmission line and the surface temperature of ceramics were introduced into the monitoring system already developed by use of LabVIEW. By using the data, the gas cooling system can automatically select the feedthrough which needs to be cooled. The solenoid valve of the selected feedthrough is operated automatically in keeping the filling gas pressure in the setting range. Figure 13 shows the outline of the gas cooling system for ceramic feedthrough. The remaining problem is that the gas is supplied from gas cylinders. Thus, it is still necessary to monitor the remaining amount of the gas in the gas cylinder and to exchange the empty cylinder.

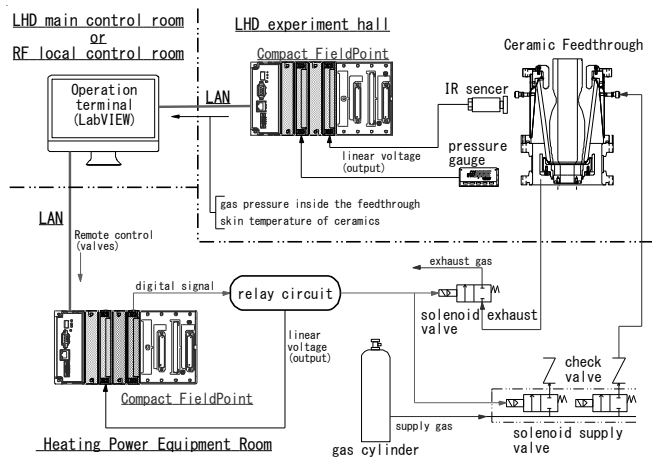


Fig. 13. Outline of the gas cooling system for ceramic feedthrough

(3) NBI

(a) The operation and maintenance of NBI in the 18th experimental campaign of LHD

The main topic of the NBI team was the BL-4 upgrade (Figure 14). In this campaign, BL-4 received a new ion-source and additional power supply for ion acceleration (20kV), and its beam-line vacuum vessel (beam dump, bending magnet, neutralizer, etc.) was reconstructed. As a result, BL-4 was upgraded to a P-NBI system of

60keV-9MW (with 4 ion-source by D-beam) from a P-NBI system of 40keV-6MW.

Figure 15 shows the shot-history of total injection beam power of N-NBI (BL-1, 2, 3). Approximately 5,200 shots of beams were injected into LHD plasma in this campaign. The maximum total injection power of N-NBI was 14.2MW due to leak troubles of BL-2 and BL-3. BL-1, BL-2, and BL-3 maintained 5.0-6.0MW, 3.0-4.3MW, and 2.0-4.0MW for plasma heating, respectively. The maximum total injection power of P-NBI (BL-4, 5) was 12.5MW. BL-4 and BL-5 maintained 3.0-6.5MW and 5.0-6.2MW, respectively, and covered a broad range of injection power as a plasma diagnostics-beam.

In this campaign, important troubles occurred at BL-2 and BL-3. One was a water leak from the Cu ground-grid of the ion-source, and another was an air leak from the H₂ gas and Cs vapor inlet port (ICF34) of the ion source. The causes were cracks on the electron beam welding part and the silver solder part. A number of minor troubles (control error, power supply error, etc.), which could be restored in a short time, were at the same level as previous experimental campaigns.

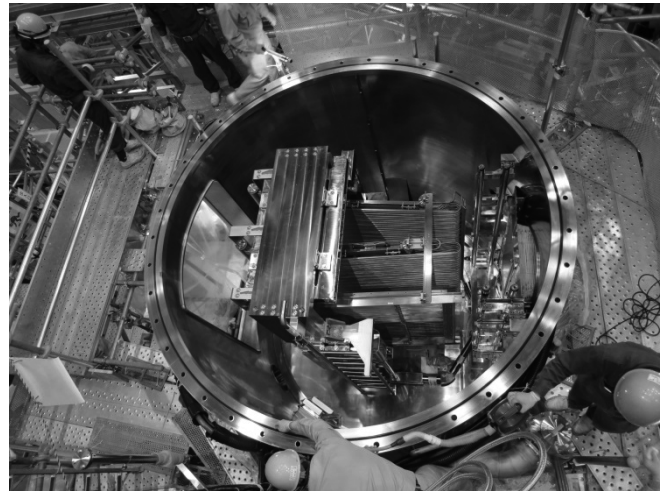


Fig. 14. The reconstruction of BL-4

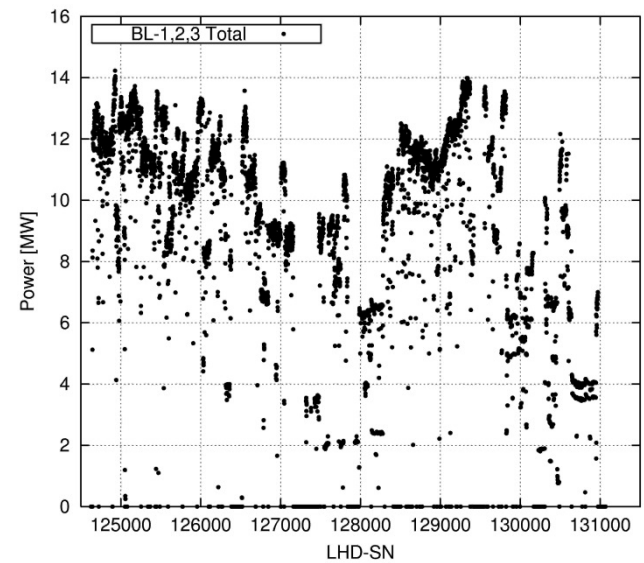


Fig. 15. The shot-history of N-NBI injection beam power

(b) Development of high energy particle analyzer with FPGA

To identify the interaction between high energy particles and Alfvén wave, we developed a pulse analyzer by high speed digitizer. The maximum sample rate is 50 megasample/sec, and it is too fast to save all raw data to PC in real time. Thus, we installed a new preprocessing system with the NI FlexRIO Field Programmable Gate Array (FPGA) module. The program for the FPGA is built via the NI LabVIEW software. Eight pulse signals of high energy particle detectors are processed in real time, and the pulse detection time, pulse height, pulse width, and pulse area for every pulse are evaluated and recorded in the data storage connected to the controller PC for NI FlexRIO. The wave forms of Alfvén wave are also recorded. A program for the automatic data viewer with the frequency spectrogram for Alfvén wave and graphs of pulse data was written. The post-processing program to evaluate phase relation of the pulse detection time with respect to the Alfvén wave was also written. The analyzed data can be recorded in the ASCII file and an image file (Figure 16).

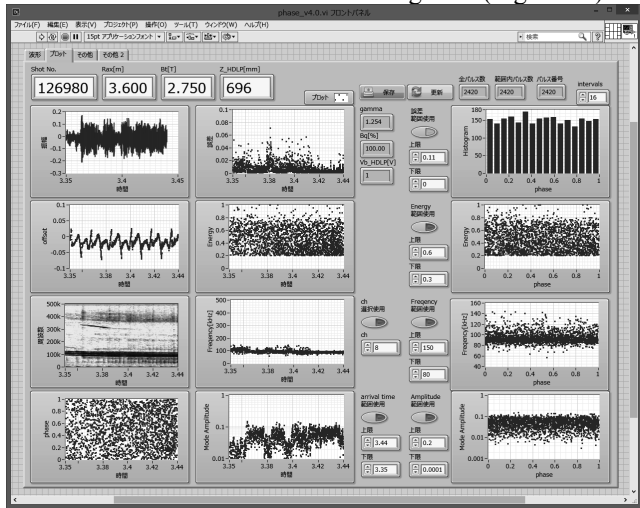


Fig. 16. An image file of the post-processing program

In the 18th experimental campaign, the measurement system ran without any trouble.

(c) Evaluation of neutral beam injection power

The Neutral Beam (NB) injected power is evaluated from the temperature rises of Calorie-Meter Arrays (CMAs), which are installed in armor tiles at the counter wall of NB injection-ports. The temperatures of CMAs are measured by thermocouples via isolation amplifiers using the WE data acquisition system. The maximum NB-injection powers, which were evaluated by the CMAs, are shown for the LHD 18th experiment campaign as follows. Here, NBI, SN, and TP mean NB Injector, Shot Number, and the duration time of NB-injection, respectively.

- BL-1 6.26MW SN=128520 TP=0.96sec
- BL-2 4.77MW SN=129331 TP=0.73sec
- BL-3 4.49MW SN=125215 TP=0.98sec

The NB injection efficiency is estimated from the evaluated NB injection power by the CMAs and the power obtained from the acceleration power supplies of the injector.

Here, monitor signals of power-supply outputs are acquired by the CAMAC data acquisition system. The injection efficiency is defined as the ratio of the injection power to the acceleration one. The typical estimated efficiencies for three tangential NBIs during the 18th experimental campaign were 0.36 for BL-1, 0.32 for BL-2, and 0.38 for BL-3.

(4) Motor-Generator (MG)

The Motor-Generator is used to supply the pulsed power to the NBI and the ECH for LHD. The MG generated 24,694 shots this fiscal year, and 575,667 shots since its construction. The operation time was 1,246 hours during this fiscal year and 26,830 hours in total.

Last year, collector rings fell into disrepair. The collector rings were polished as a temporary repair. In addition, we strengthened monitoring of collector rings and brushes. Figure 17 shows the length of brush abrasion in this fiscal year. Abrasion of motor brushes was too great because these collector rings were uneven. It is necessary to change brushes every two experimental campaigns. We wish to repair the collector rings with an overhaul of the MG.

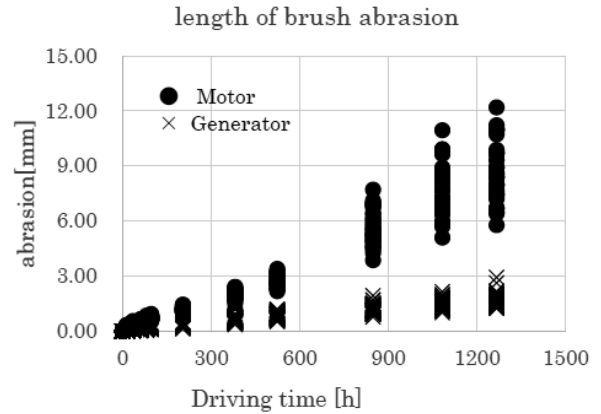


Fig. 17. Trend of collector brush abrasion

4. Diagnostics Technology Division

This division supports development, operation, and maintenance of diagnostic devices for the LHD.

We support development and construction of fusion products diagnostic system and its calibration system for the deuterium experiments of the LHD. We are also preparing several kinds of radiation measuring equipment to ensure the safety of the experiments. And we are measuring and compiling data of environmental radioactivity in the LHD building and neighboring areas to estimate the influence from the deuterium experiments in the future.

We also support operation and maintenance of diagnostic devices such as the FIR, Microwave Reflectometer, Thomson scattering diagnostic, the HIBP, and others. We also carried out the preliminary vacuum leak tests on several diagnostic devices. And in order to store the extremely huge data from these diagnostics, new 4 RAIDs have been set up in the LHD data storage system.

Our principal tasks during this fiscal year are described below.

(1) Fusion products diagnostics system

The fusion products diagnostics system, a wide range neutron flux monitor (NFM), a neutron activation foil system (NAS), and radial neutron cameras (RNC) have been installed primarily on the LHD in preparation for the deuteron operation.

NFM is essentially required in terms of both plasma physics and radiation safety. NFM consists of detector sets, pre-amplifier, and the digital-signal-processing (DSP) unit. Three NFMs have been installed in the LHD torus building, as shown in Figure 18. Because the cable between the detector and the pre-amplifier of the fission chamber has been limited up to about 40 m, the pre-amplifiers are located in the basement of the torus hall. The DSP units are located in the diagnostics room (2), which is isolated by a concrete wall 2 m thick from the torus hall.

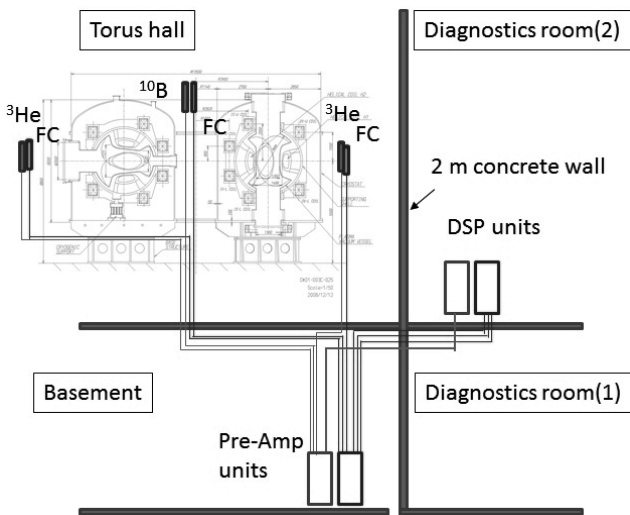


Fig. 18. Arrangement of NFM system

NAS consists of capsule packing neutron activation foil, capsule sending unit, electromagnetic valve unit, and tube and chamber transferring capsule within sight of plasma. Figure 19 shows capsule sending units located in measurement room (1) and the electromagnetic valve units located in the compressor room, respectively.

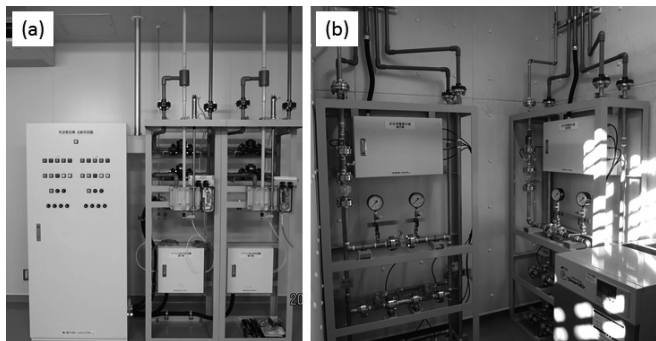


Fig. 19. (a) Capsule injector units and control panel. (b) Electro-magnetic valve units.

RNC consists of stilbene scintillation detectors maximized in the counting rate capability and multichannel collimator unit with apertures of 26 channels with 1.5 m length. The collimator unit has been made by heavy concrete with the specific gravity of above 3.5 using hematite as the main material. This unit has been installed in the open mouth with 2 m depth on the floor of the torus hall, as shown in Figure 20.

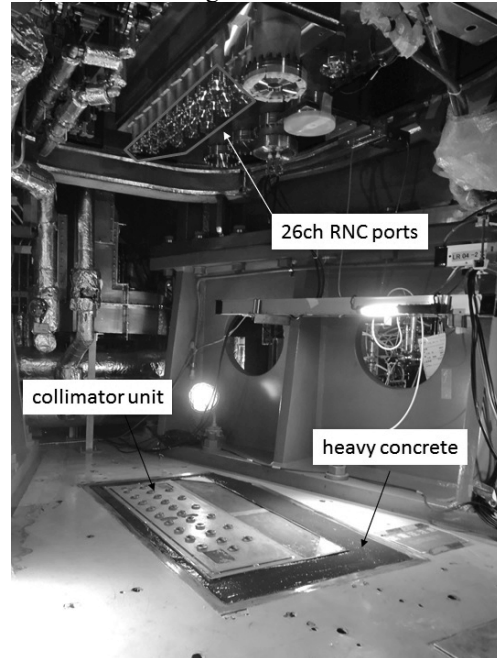


Fig. 20. Multichannel collimator installed in floor aperture.

(2) Radiation Monitoring

For comparison in the future, we are measuring and compiling data of environmental radioactivity in the LHD building and neighboring areas. We are doing maintenance of several radiation measuring instruments to measure environmental radioactivity as below.

(a) High-Purity Germanium (HPGe) Detector

Some samples of soil or pine needles in the NIFS site are measured with the HPGe detector (Figure 21) to search spectrum data and nuclides. Filters of the radiation gas monitors are also measured with the detector. We confirm whether this detector operates correctly by using Co-60 one time each month.

Another detector was added to measure neutron activation foils.

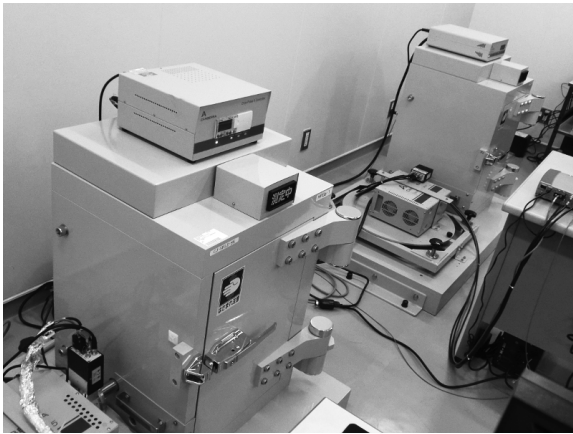


Fig. 21. High-purity germanium (HPGe) detector

(b) Gas and Water Monitor

By continuing environmental radioactivity measurements, gas and dusts in the torus hall and in exhaust from the LHD building, and drain water have been measured continually. The operation and maintenance procedures of the measuring instruments have been established. The procedures for daily check has been compiled in a manual. Shown in Figure 22 is the water outlet for collecting the drained water.



Fig. 22. Before drainage, water is sampled manually and measured with a low background liquid scintillation counter (LSC-LB7).

(3) Integrated Radiation Monitoring System

In order to integrate information for radiation safety, an integrated radiation monitoring system is planned. Figure 23 shows the schematic diagram.

This system retrieves data from a variety of radioactivity measurements, the access control system, and ITV cameras. In the event of high-dose radiation, an error of radioactivity measurements, or the opening of a door which must remain closed, this system stops the LHD experiment automatically.

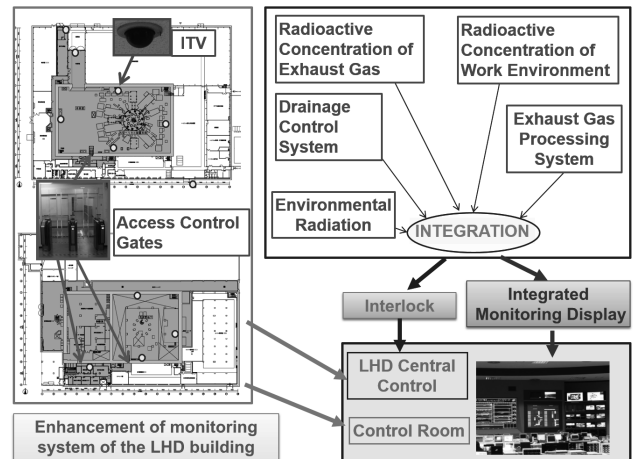


Fig. 23. Schematic view of the integrated radiation monitoring system

(4) Operation and Maintenance of Diagnostics Devices

The operation and maintenance (for example, high voltage power supply, vacuum pumping system, supplied gas system, phase detection circuit, dehydrator, water cooling system etc.) were responsibly executed.

We supported reforming and shielding the laser path of FIR and Thomson scattering diagnostics for the deuterium plasma experiments.

We also made a neutron shelter for the HIBP by way of trial for the deuterium experiment. In order to facilitate access to the device, shielding blocks are divided into suitable units. Each shielding block is fixed with only one bolt (Figure 24). It is possible to install additional shielding (lead, etc.) if needed.

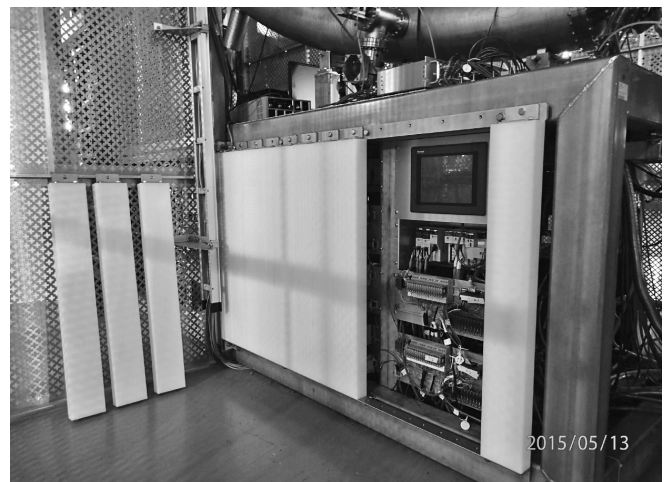


Fig. 24. Prototype of neutron shielding for the HIBP

(5) Vacuum Leak Test Chamber in the Plasma Diagnostics Laboratories

The vacuum leak test chamber is maintained well and the preliminary vacuum leak tests were carried out on several diagnostic devices to be used for the LHD plasma experiment. (Figure 25)

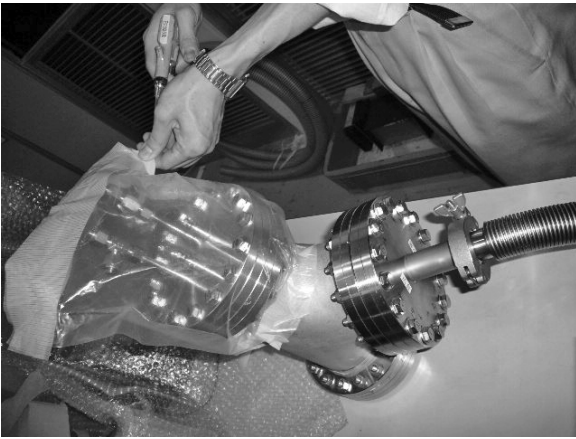


Fig. 25. Example of tested devices (ICF152)

(6) LHD Data Storage System

For the LHD data storage system, the new 4 RAID5s have been set up to store the 18th campaign data of the LHD plasma experiments. (Figure 26) These are managed by the “GlusterFS” file system and provide one huge storage volume. Additionally, all data in the past on the old RAID5s using fiber channel I/F have been moved into the new volume. Consequently, we are preparing to remove all the old RAID5s and the fiber channel switch.

For preparing the deuterium experiments, the “remote power manager” application is under development. This application has GUI and has been developed in C#, and it can help the operators monitor the state and the on-off status of the power of each PDU (Power Distribution Unit) remotely.

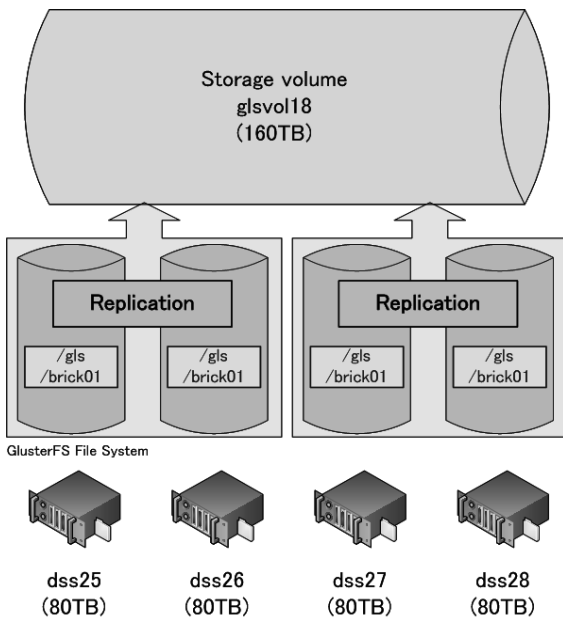


Fig. 26. Data Migration Procedure

5. Control Technology Division

The Control Technology Division contributed to important technological aspects of the LHD, such as operation and management, and development of the system.

The division contributed also to management of the network system. The work in system operation and system management is as follows: operation of the cryogenic system and the power supply system for the superconducting coils, updating the central control system and cryogenic control system, and management of the network system. The work in system development this year is as follows: development of a new simulation algorithm for the cryogenic system, system development of the control system for LHD, and others. Details of the activities in this division are described below.

(1) Operation of the LHD superconducting system

LHD cryogenic system operation was started on September 25, 2014, in the 18th experimental campaign, and helium gas was purified for impurities removal as usual. The coil cool-down was started on October 8, and it was completed on November 4. The number of steady-state operation days of the superconducting coils was 95. Operation without serious trouble enabled implementation of the experimental plan. The coil warm-up was started on February 6, 2015, and it finished on February 27. The availability of the cryogenic system achieved 100%, and the total operation time was 3,717 hours in this campaign. (Figure 27)

The first excitation of the LHD in the experimental campaign was started on November 4, 2014, and it was finished on February 5, 2015. The number of excitation times was 56, and total operation time was 425 hours in this campaign. In these operations, the high voltage power supply for pulsed excitation was used seven times and the polarity switch device was used 14 times.

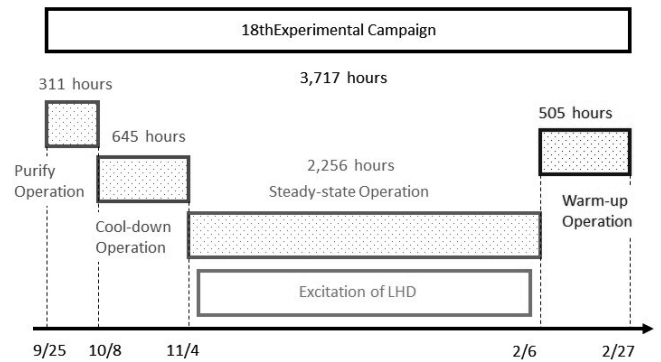


Fig. 27. Operation time of LHD cryogenic system

(2) Update of the LHD cryogenic control system

The cryogenics system ran without any trouble during this year. The total system operating time was 359 days (8627 hours). The total compressor operating time was 157 days (3784 hours).

We upgraded two systems this year. First, we removed the system from the poloidal coil local control panel for collecting vacuum pumping data, and sent it to the operation terminal. Secondly, we added a function which determines an abnormality of input data range of remote I/O.

(3) Problem report and improvement of power supplies for LHD superconducting coils

We report problems of power supply for the LHD superconducting magnets and improvements during the 18th experiment.

Each power supply control system communicates with an integrated computer using reflective memories and optical cables. The integrated computer gives orders to each power supply control system and controls six power supplies. When a problem occurs, the integrated computer sends a failure signal to the central control system. Figure 28 shows the system block diagram.

During the 18th experiment, a communication error occurred because the integrated computer froze, and each power supply control system lowered the current by itself. Figure 29 shows the current waveform of the coils of the LHD. When a problem occurs, usually the integrated computer sends a failure signal. Then the central control system stops the experiment immediately. But in this case, the failure signal was not sent because the integrated computer froze. Therefore, the experiment continued for a period of time though the current was descending.

It is a significant problem that we cannot detect power supply problems immediately. Therefore, we added signal wiring to send signals to the central control system even if the integrated computer freezes. Figure 30 shows the additional wiring diagram. We could keep the experiment safe by this improvement.

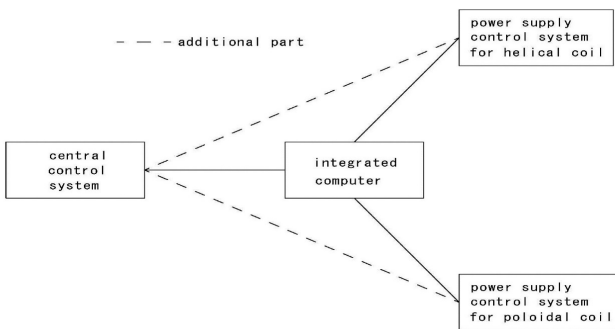


Fig. 28. System block diagram

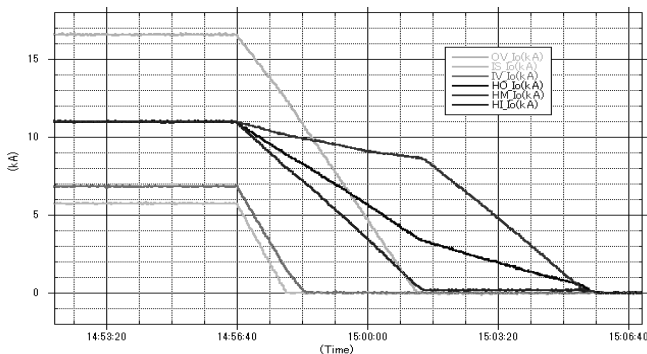


Fig. 29. Screen displaying waveform

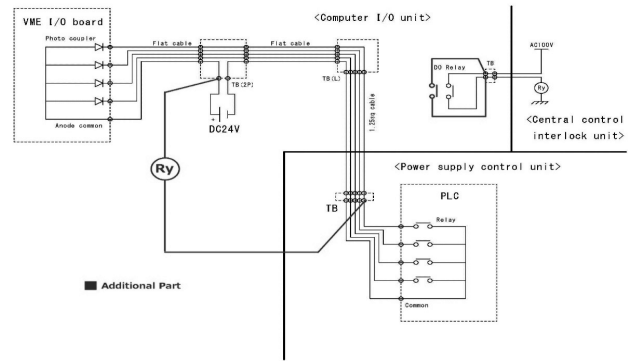


Fig. 30. Additional wiring diagram

(4) Update of the LHD central control system

Two Exhaust Gas Processing Systems were installed in the LHD building. These systems have an interlock that connects them and the central control system with the signal line.

In order to integrate the information for radiation safety, the integrated radiation monitoring system was planned. The connection was examined between this system and the LHD central control system.

(5) Network management

The NIFS campus information networks consist of several clusters. We manage the Research Information Cluster (NIFS-LAN) and the LHD Experiment Cluster (LHD-LAN).

(5.1) NIFS-LAN

NIFS-LAN is the network of general use, and covers the entire area of the campus. We have administrated the Routers, layer-2 / layer-3 switches, the quarantine authentication system, the Mail server, the SSL-VPN server, the DNS server, and the DHCP server.

New contributions in FY 2014 are as follows:

(a) Introduction of the quarantine authentication system

The quarantine system has been introduced for security improvement. The security check is automatically conducted when the user connects a PC to an information outlet and then the PC is connected to the pre-specified VLAN. MAC address registration is needed for all PCs. The guest user can connect a PC to the external network without registration. This system began operation in September 2014. Information from approximately 1600 terminals is registered with the database.

(b) Renewal of the mail system

The DEEPSOFT mail system was replaced by MailSuite (Figure 31). This system works on the virtual system, and has multiple functions consisting of a mail server, an Anti-SPAM filter, and a mailing list server.

(c) Distribution of the SEP version 12.1.5

We started to distribute the Symantec Endpoint Protection (SEP) version 12.1.5, which covers the Windows 8.1, Windows Server 2012, and MacOS X 10.10.

(d) Upgrading the operating system of SSL-VPN server

The operating system of SSL-VPN server was upgraded in order to make remote access service available to the new OS, such as MacOS X 10.10 and newer versions of security software.



Fig. 31. Webmail window of the new mail system

(5.2) LHD-LAN

The LHD-LAN has been contributing to the LHD experiments since 1996. The new “LHD-LAN Core Switch System” was renewed in fiscal years 2007-2008. The main part consists of two Cisco Catalyst 4507R multi-layer switches connected by 10 Gbps Ethernet, whose maximum throughput is over 210 million packets per second.

(a) LHD Access Gateway

A firewall was installed to limit the connection between NIFS-LAN and LHD-LAN, and MAG4610 (Juniper Network) is operated as the authentication server.

We dealt with user account management (30 initial registrations in FY2014), information alteration of the security policy of the Windows OS, inquiries from users, etc. In order to fix some difficulties of MacOSX10.9.x, we asked the manufacturer.

(b) Wireless LAN examination in the LHD room during the experiment

We tested the wireless LAN in the LHD room during the experiment. Figure 32 shows the placement of the wireless LAN. As a result of the test, packet loss increased drastically day by day by energizing of the magnetic field, and finally it reached 100% loss. In addition, the access point did not respond. From these results, we use a cable.

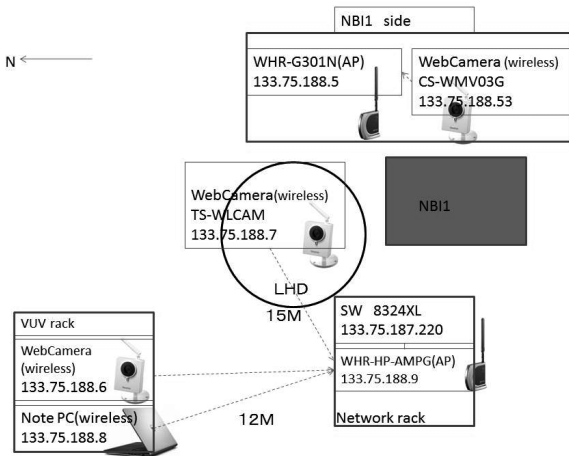


Fig. 32. Placement of wireless LAN

(6) Updating the control systems for instruments attached to the LHD

We developed some remote control programs used for the system for the LHD experiment. The Boronization control software is based on old Windows NT. The HIBP control program needs a new program for communication. On the other hand, we also developed a control program for TESPEL (TESPEL2) because this system is a new installation.

These programs were developed with a template based on WPF (Windows Presentation Foundation) by Microsoft. Figures 33 and 34 show the controllers. This WPF has many versatile functions, such as checking and showing the condition of PLC periodically, connecting using TCP or RS-232C, logging automatically, and showing trend graphs. It also can be used for similar remote control programs or other measurement programs.

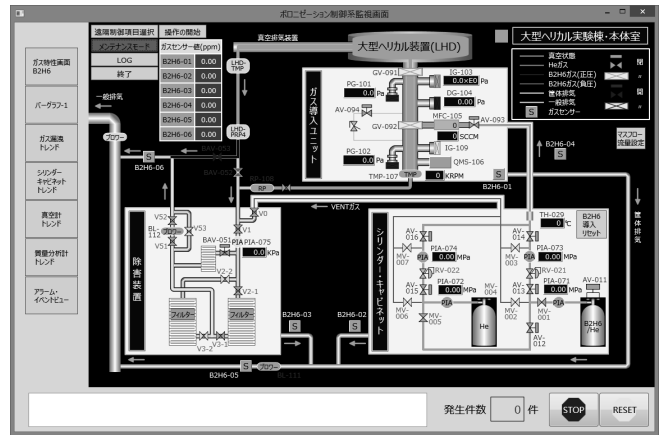


Fig. 33. Boronization controller

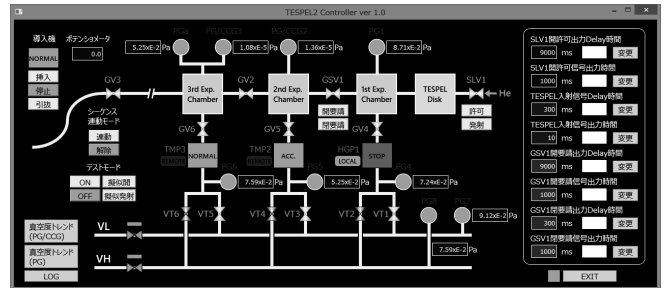


Fig. 34. TESPEL2 controller

(7) Modeling and simulation of SHe loop of the Central Solenoid coil (CS) in ITER cryogenic system by C-PREST

In a Tokamak, the plasma current is induced by pulse operation of the CS. At that time, a heat load of 1.3 MJ for two seconds is generated in the CS by AC losses. To investigate the impact of pulsing heat load on the SHe loop of the CS, we implemented modeling and conducted dynamic simulation. Figure 35 shows a schematic diagram of the SHe loop of CS, which consists of two heat exchangers immersed in a liquid helium (LHe) reservoir, a circulation pump (CP), and bypass valves for flow distribution. The CS composed of six modules is formed by using a superconductor (SC) unit module. The SC unit module was developed based on a pipe unit module, and was validated by comparison with a CS model coil experiment data from JAEA.

Figure 36 shows a simulation result of the SHe loop of the CS under 15 MA baseline scenario. The amplitude of heat load is about 9kW. However, it is possible to maintain the stable operation. The effect that the substantial heat load gave to the SHe loop of the CS was limited. And it was confirmed not to need special protected sequence operation for CP. Consequently, the SHe loop of the CS can maintain the operating conditions of the stable SC coil at the time of the DT plasma operation.

Ohmine (Okinawa National College of Technology) September 1-5, 2014, and Mr. Miyata (Tottori University) December 4-5, 2014. And the meeting “Symposium on Safety and Health Management in a Laboratory” was held February 5-6, 2015, with 50 participants from 15 universities and four institutes.

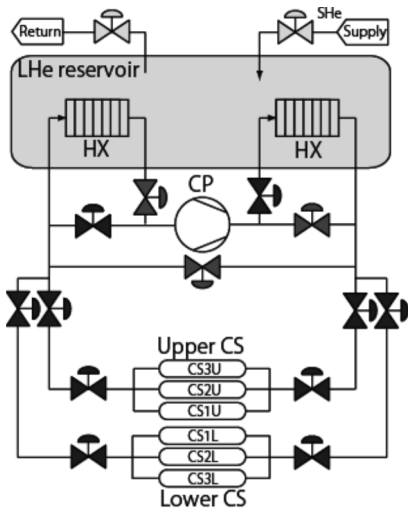


Fig. 35. Schematic of the SHe loop of the CS

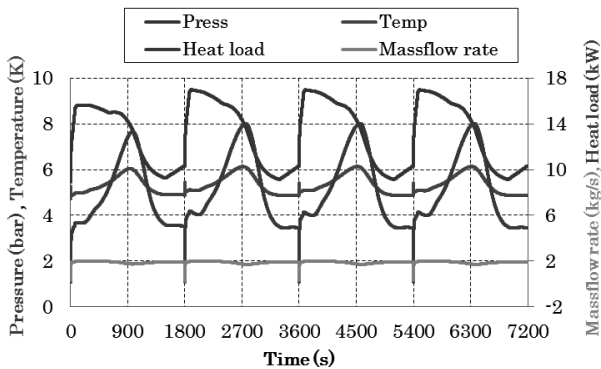


Fig. 36. Simulation result at the outlet of the SHe pump

6. Symposium on Technology, Technical Exchange and Dual System

(1) The Symposium on Technology

The Symposium on Technology was held September 4-5, 2014, at Hokkaido University. There were 783 participants from many Japanese universities, national laboratories, technical colleges, and industries.

At this symposium, 405 papers were presented in 12 oral sessions and poster sessions. Technical experience and new techniques were reported and discussed. Our department presented five papers.

(2) Technical Exchanges

Technical exchanges between our department and other institutes or universities were held in order to improve the technical skills of the staff. In this FY, we invited Mr.